JOURNAL OF SOLID STATE CHEMISTRY **129,** 242–249 (1997)
ARTICLE NO. SC967223

Structural Stability of the 1T Structure on Transition-Metal Dichalcogenides

I. Compounds in the NbS_2–IrS_2 System

M. Shimakawa, K. Kawachi, S. Nishikawa, and K. Hayashi

Laboratory for Solid State Chemistry, Okayama University of Science, 1-1 Ridai-cho, Okayama 700, Japan

Received July 15, 1996; accepted November 12, 1996

A new family of the 1T compounds is prepared in the NbS_2–IrS_2 system and the $NbSe_2$–$IrSe_2$ system. The end members of the above systems do not crystallize into the 1T structure. In the NbS_2–IrS_2 system, the structure variation from the $2H_a$ structure to the pyrite structure through 1T structure has been observed as the average number of the valence electrons per atom increases. Also, in the $NbSe_2$–$IrSe_2$ system, the structure variation from the $4H_a$ structure to the pyrite structure through 1T structure has been observed as the average number of the valence electrons per atom increases. The relative structural stability of the 1T structure in comparison with the $2H_a$ and the pyrite structures is discussed. The electrical resistivity has been measured from room temperature to 30 K, and the magnetic susceptibility has been measured from room temperature to 5 K. The 1T compounds of those systems show semiconductive and weak-paramagnetic behavior. © 1997 Academic Press

INTRODUCTION

The 1T structure is the same as the so-called "CdI_2 structure," constructed with octahedraly coordinated metal atoms. The 1T structure has been observed in the transition-metal disulfides of the Ti (1), Zr, Hf (2), Ta (3), and Pt (4); in the transition-metal diselenide of the Ti (5), Zr (6, 7), Hf (8), V (9, 10), Nb (11), Ta (12), and Pt (4); and in the transition-metal ditellurides of the Ti (13), Zr (14), Hf (15), V (16), Nb, Ta (17), Ni (4), Co (18), and Pt (4). Concerning the transition-metal disulfides and the diselenides, the 1T structure is stabilized only in the $nd^2(n+1)s^2$-, $nd^3(n+1)s^2$-, and $nd^8(n+1)s^2$-transition-metal dichalcogenides. The relative orbital energies of the metal atom nd and $(n+1)s$, and that of the p of the chalcogen atom, are important in considering the relative structural stability of the 1T, 2H, and pyrite structures. However, roughly speaking, if four electrons transfer from a metal atom to two chalcogen atoms at the formation of a compound, the state of the filled chalcogen p-bands and the empty metal d-bands for the $nd^2(n+1)s^2$-transition-metal dichalcogenides lowers the electron energy of the compounds because of the wide band gap between the filled band and the empty band. The same also occurs for the state of the filled chalcogen p-bands, the filled metal t_{2g}-bands and the empty metal e_g-bands for the $nd^8(n+1)s^2$-transition-metal dichalcogenide.

The $nd^4(n+1)s^2$-transition-metal dichalcogenide favors the 2H structure constructed with the trigonal prismatic coordination of the metal atom. The chalcogen p band and the metal d_{z^2} band are filled with electrons and the other metal d bands are empty in the $nd^4(n+1)s^2$-transition-metal dichalcogenide. Thus, the energy of the electrons is lowered in the $nd^4(n+1)s^2$-transition-metal dichalcogenide and the 2H structure constructed with the metal atom of the trigonal prismatic coordination is stabilized. The 2H structure has been observed in the transition-metal disulfides and diselenides of the Nb (19, 20), Mo (21, 22), Ta (23–26), and W (27–30).

The $nd^3(n+1)s^2$-transition-metal dichalcogenide favors both the 1T structure constructed with the metal atoms of the octahedral coordination and the 2H structure constructed with the metal atoms of the trigonal prismatic coordination. However, the vanadium dichalcogenides favor the 1T structure, and the niobium disulfide favors the 2H structure constructed with the metal atoms of the trigonal prismatic coordination. The $NbSe_2$, TaS_2, and $TaSe_2$ crystallize into both the 1T structure and the 2H structure.

The pyrite structure is observed on the transition-metal disulfides of Mn (31), Fe (32, 33), Co (32), Ni (34, 35), Cu (36), Zn (34), Ru, Os (37), and Ir (38, 39), on the transition-metal diselenides of Mn (40), Fe (34), Co, Ni (35), Cu (41), Zn (34), Ru (42), Rh (43), Os (37), and Ir (39, 44), and on the transition-metal ditellurides of Mn (31), Fe (34), Ru (45), Rh (46), Os (37), and Ir (47). The essential feature of pyrite is that the diatomic sulfurs accept two electrons from a metal atom at the formation of the compound. Consequently, roughly speaking, the stability of the divalence state of the metal atom is important for the structural stability of

0022-4596/97 $25.00

the pyrite structure. The band splitting between t_{2g} and e_g should be large and the relative energy level of the metal d band and chalcogen p band should be close for stabilizing the pyrite structure (48).

It is very hard to predict the structural stability between the 2H structure and the pyrite structure on the basis of the above hypothesis. Therefore, it is necessary to confirm the structural relation of the 2H structure and the pyrite structure. The 2H structure of the transition-metal dichalcogenides and the pyrite structure are mostly stabilized with niobium, which, in turn, is just before the $nd^4(n+1)s^2$-transition-metal atom and the iridium atom, which is just after the $nd^6(n+1)s^2$-transition-metal atom. Consequently, the 2H structure and the pyrite structure will appear in the Nb–Ir–ch system (ch: chalcogen). The phase diagrams of the NbS_2–IrS_2 and $NbSe_2$–$IrSe_2$ systems are studied. Especially, the homogeneity range of the 1T phase found in the present investigation was precisely determined. The electrical resistivity of the samples with the 1T structure was measured from room temperature to 30 K. The magnetic susceptibility was measured from room temperature to 5 K.

EXPERIMENTAL DETAILS

Sample Preparation

The starting materials, the Ir powder (99.9% pure; Mitsuwa), the Nb powder (99.9% pure; Mitsuwa), S blocks (99.9999% pure; Wako), and Se shot (99.999% pure; Aldrich) are sealed in an evacuated quartz ampoule. The ampoule is heated at 1000°C for 2 days to complete the reaction and then it is annealed at the desired temperatures between 700 and 1000°C for 1 week. Then the sample was obtained after quenching the ampoule in water.

Chemical Composition Analysis

The chemical compositions of the samples are analyzed with an electron probe microanalyser (EPMA) by the ZAF method. The Nb, L line; the Ir, M line; the S, K line; and the Se, L line are used for the composition analysis.

Crystal Structure Determination

The sample powder was processed with an acetate glue to avoid the preferred orientation on the measured powder X-ray diffraction pattern. After drying and grinding, the sample was mounted on the sample holder and the X-ray diffraction on the processed powder was measured (49). Data were taken for 2 s at each 2θ step of 0.05° from 29 to 80°. The crystal structure parameters were refined by the Rietveld method using the computer program RIETAN (50).

X-Ray Photoelectron Spectra

The X-ray photoelectron spectra of the core levels were measured on the pressed samples using a Shimazu ESCA 850 spectrometer. Mg$K\alpha$ radiation was used for the X-ray source and the FWHM was 1.0 eV. The measurements were repeated 100 times for each sample. The energy values of the spectra were calibrated in each measurement with the carbon $1s_{1/2}$ peak (285 eV).

Magnetic Susceptibility Measurement

The magnetic susceptibility was measured from 5 to 300 K on the powder sample by the SQUID method. The applied magnetic field was 10,000 G.

Electrical Resistivity Measurement

The electrical resistivity was measured on the pressed powder samples by the van der Pauw method in the temperature range of 30–300 K.

RESULTS AND DISCUSSION

NbS_2–IrS_2 System

In the present investigation, the phase relations of the NbS_2–IrS_2 system were studied in the temperature range of 700–1000°C. A phase diagram of the system is shown in Fig. 1. It was found that the homogeneity range of the 1T phase spreads over the composition range between 6 and 50 mol% IrS_2 at 1000°C. The homogeneity range of the 1T phase becomes narrow at low temperatures. The two-phase region, 1T + IrS_2, lies between 50 and 99 mol% IrS_2. The other two-phase region, 1T + $2H_a$, lies in the narrow composition range near NbS_2.

Usually, the 1T phase is observed in the mixed transition-metal dichalcogenides in which at least one of the end member transition-metal dichalcogenides is the 1T phase. However, in the $Nb_{1-x}Ir_xS_2$, the end member NbS_2 does

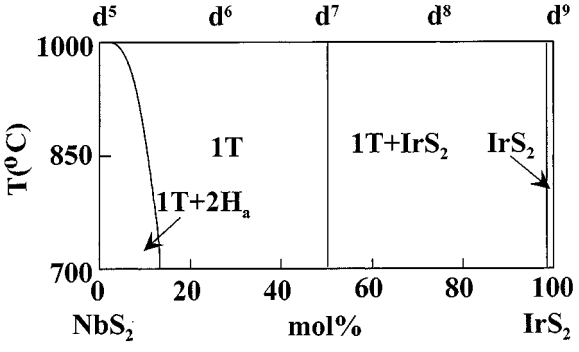

FIG. 1. Phase diagram of the NbS_2–IrS_2 system.

not crystallize into the 1T structure, but the other end member IrS_2 crystallizes into the pyrite-like structure. Therefore, the 1T structure of the $Nb_{1-x}Ir_xS_2$ is the 1T structure of the new concept. The structural stability of the new concept 1T phase will be discussed in a later chapter.

The lattice parameters and the axial ratio, c/a vs chemical composition for the 1T-$Nb_{1-x}Ir_xS_2$ are shown in Fig. 2. Around $x = 0.3$, the a parameter shows the minimum, and the c parameter and the axial ratio c/a show the maximum.

For the samples of 1T-$Nb_{1-x}Ir_xS_2$, the atomic positions and temperature factors are listed in Table 1. We consider that the Ir atoms and Nb atoms of the $Nb_{1-x}Ir_xS_2$ occupy the same sites statistically. The observed profile, the calculated profile, and the difference profile of the powder X-ray diffraction of 1T-$Nb_{0.925}Ir_{0.075}S_2$ are shown in Fig. 3. The final R.I value is 0.018. No extra peaks are observed in the powder X-ray diffraction pattern.

TABLE 1
Atomic Position and Temperature Factors of 1T-$Nb_{1-x}Ir_xS_2$

x	z^a	B_j for (Nb, Ir)	B_j for S
0.063	0.260(2)	1.55	1.04
0.075	0.260(2)	1.51	0.88
0.100	0.259(1)	1.95	1.18
0.130	0.259(1)	2.14	0.66
0.150	0.255(2)	2.53	1.69
0.250	0.254(2)	2.58	1.72
0.500	0.246(4)	2.13	1.08

Note. Space group $P\bar{3}m1$ (No. 164), $Z = 1$. Atomic position (Nb, Ir) in 1(a): (0, 0, 0); S in 2(d): $\pm$ (1/3, 2/3, z).
[a] z position of S.

$NbSe_2$–$IrSe_2$ System

The phase relations in the $NbSe_2$–$IrSe_2$ system are studied in the temperature range between 800 and 1000°C.

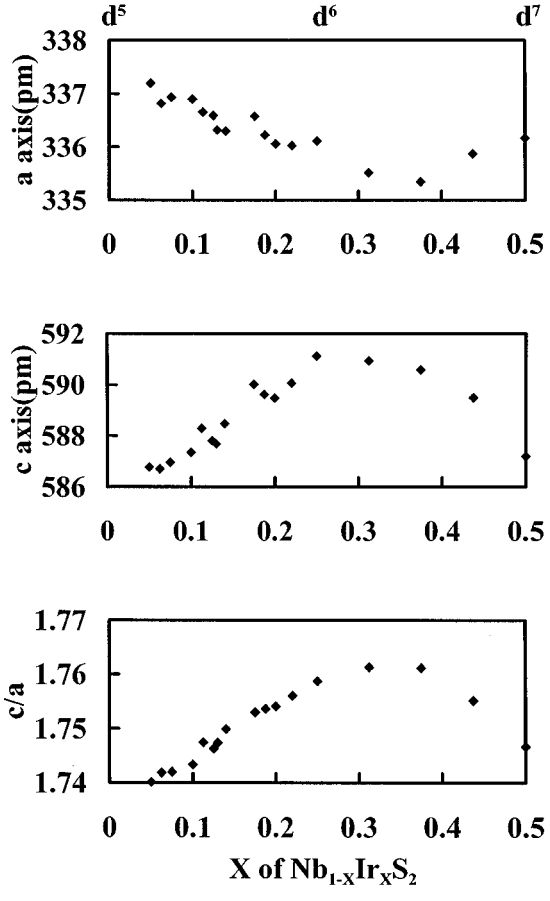

FIG. 2. Lattice parameters and axial ratio vs chemical composition for 1T-$Nb_{1-x}Ir_xS_2$.

For $NbSe_2$, the seven polytypes, 1T, $2H_a$, $2H_b$, 3R, $4H_a$, $4H_{d1}$, and $4H_{d2}$ have been reported by Kadijk and Jellinek (11), Marezio *et al.* (52), and Furuseth *et al.* (53). It is known that the 1T, $4H_{d1}$, and $4H_{d2}$ polytypes are not quenchable. Also, it is known that the crystal structure of $IrSe_2$ is the same as that of IrS_2. In the present investigation, 1T and $4H_a$ polytypes and $IrSe_2$ structure are observed in the $NbSe_2$–$IrSe_2$ system.

The phase diagram of this system is shown in Fig. 4. The homogeneity range of the 1T phase spreads over the composition range between 8 mol% $IrSe_2$ and 42 mol% $IrSe_2$ at 1000°C. The $4H_a$ phase is observed near $NbSe_2$. A two-phase region of the 1T + $IrSe_2$ lies on the composition range between 42 mol% $IrSe_2$ and 99 mol% $IrSe_2$. The other two-phase region, 1T + $4H_a$, lies on the composition range between 5 mol% $IrSe_2$ and 7 mol% $IrSe_2$.

The lattice parameters and the axial ratio c/a vs chemical composition for the 1T-$Nb_{1-x}Ir_xSe_2$ are shown in Fig. 5. Around $x = 0.3$, the a parameter shows the minimum, and the c parameter and axial ratio, c/a, show the maximum. These features of the lattice parameters of $Nb_{1-x}Ir_xSe_2$ are similar to those of $Nb_{1-x}Ir_xS_2$.

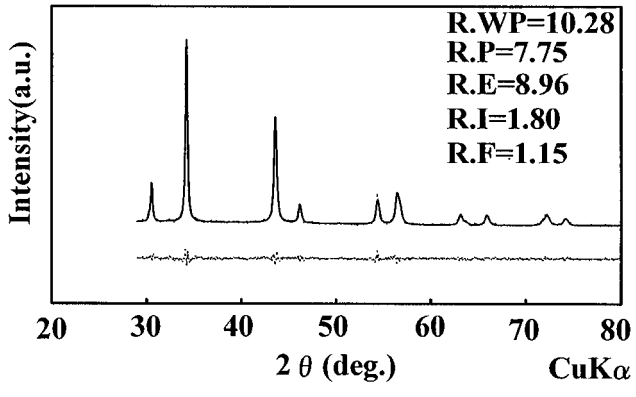

FIG. 3. Observed, calculated, and difference profiles of 1T-$Nb_{0.925}Ir_{0.075}S_2$.

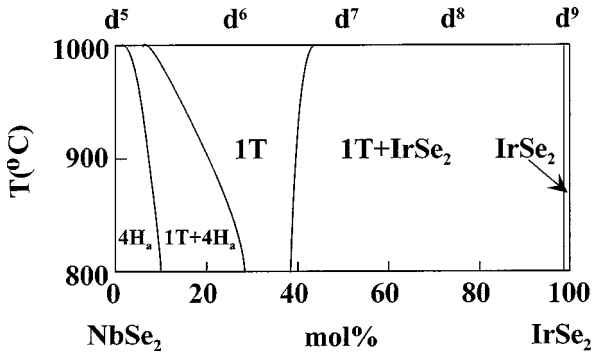

FIG. 4. Phase diagram of the $NbSe_2$–$IrSe_2$ system.

The atomic position parameters and temperature factors of $Nb_{1-x}Ir_xSe_2$ are listed in Table 2. The Ir and Nb atoms occupy the same sites statistically. The observed profile, the calculated profile, and the difference of the X-ray diffraction patterns of 1T-$Nb_{0.80}Ir_{0.20}Se_2$ are shown in Fig. 6. The final *R*.I value is 0.02. No extra peaks are observed in the X-ray diffraction pattern.

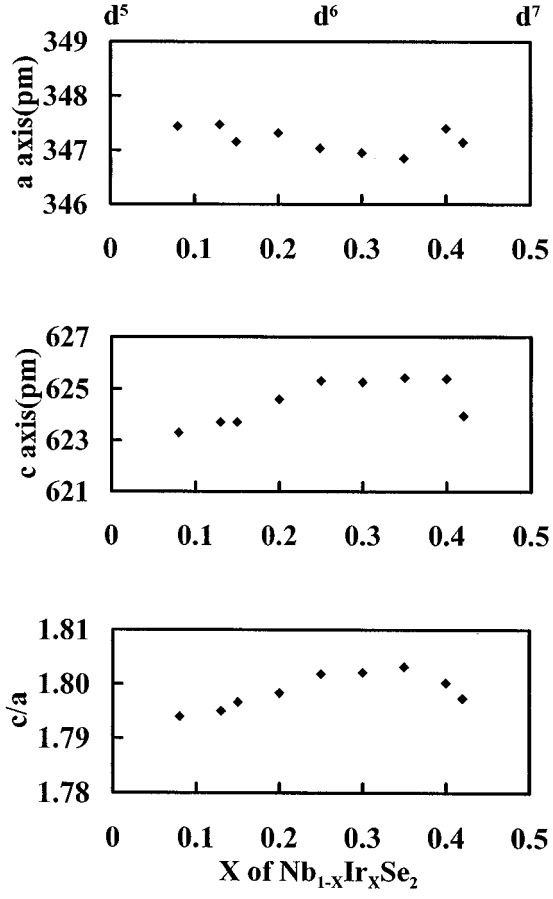

FIG. 5. Lattice parameters and axial ratio vs chemical composition for 1T-$Nb_{1-x}Ir_xSe_2$.

TABLE 2
Atomic Position and Temperature Factors of 1T-$Nb_{1-x}Ir_xSe_2$

x	z^a	B_j for (Nb, Ir)	B_j for Se
0.08	0.264(1)	2.02	1.11
0.10	0.264(1)	2.16	1.04
0.13	0.263(1)	1.98	0.74
0.15	0.264(1)	2.32	0.66
0.20	0.262(1)	2.34	1.20
0.25	0.261(1)	2.07	1.27
0.42	0.254(2)	1.99	2.16

Note. Space group $P\bar{3}m1$ (No. 164), $Z = 1$. Atomic position (Nb, Ir) in 1(*a*): (0, 0, 0); Se in 2(*d*): $\pm$ (1/3, 2/3, *z*).
[a] *z* position of Se.

The data of chemical composition analysis listed in Table 3 indicate that the composition of the compound shifts to the iridium-rich composition from the chemical composition of the initial charge by less than 5%.

X-Ray Photoelectron Spectra of 1T-$Nb_{1-x}Ir_xS_2$ and 1T-$Nb_{1-x}Ir_xSe_2$

The binding energy values of 1T-$Nb_{1-x}Ir_xS_2$ and 1T-$Nb_{1-x}Ir_xSe_2$ are listed in Table 4. The reference values of energies of the Nb metal, 3d5/2; the Ir metal, 4d5/2; the S, 2*p*; and the Se, 3*d* are 202.18 (54), 296.3 (55), 164.25 (56), and 55.2 eV (57), respectively. In 1T-$Nb_{1-x}Ir_xS_2$ and 1T-$Nb_{1-x}Ir_xSe_2$, the $Nb3d_{5/2}$ energy value was about 207 eV and the $Ir4d_{5/2}$ energy was about 298 eV. The $Nb3d_{5/2}$ binding energy value is shifted toward the high energy side by about 4–5 eV, and the $Ir4d_{5/2}$ binding energy value is shifted toward the high energy side by about 2 eV. Also, the S binding energy value is shifted toward the low energy side by about 2 eV. Therefore, we consider that the Ir, Nb, and

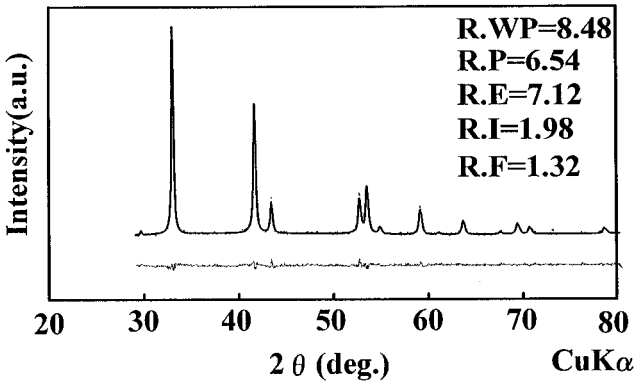

FIG. 6. Observed, calculated, and difference profiles of 1T-$Nb_{0.80}Ir_{0.20}Se_2$.

TABLE 3
Chemical Composition of $Nb_{1-x}Ir_xSe_2$

Composition of initial charge (%)			Analyzed composition (%)		
Ir	Nb	Se	Ir	Nb	Se
5.0	45.0	50	6.0	44.6	50
10.0	40.0	50	11.0	41.2	50
12.5	37.5	50	12.9	39.6	50
15.0	35.0	50	16.2	37.8	50
17.5	32.5	50	18.6	35.5	50
20.0	30.0	50	22.3	34.0	50

Note. The selenium content is fixed at 50%.

TABLE 4
X-ray Photoelectron Spectra of 1T-$Nb_{1-x}Ir_xS_2$ and 1T-$Nb_{1-x}Ir_xSe_2$

x of $Nb_{1-x}Ir_xS_2$	Nb $3d_{5/2}$	Ir $4d_{5/2}$	S $2p$
0.3125	206.7(eV)	297.3(eV)	162.3(eV)
0.175	207.0(eV)	297.6(eV)	161.6(eV)
0.150	206.5(eV)	297.3(eV)	162.2(eV)
x of $Nb_{1-x}Ir_xSe_2$	Nb $3d_{5/2}$	Ir $4d_{5/2}$	Se $3d$
0.48	207.4(eV)	297.7(eV)	54.9(eV)
0.25	207.6(eV)	297.4(eV)	54.9(eV)

S atoms in the 1T-$Nb_{1-x}Ir_xS_2$ and 1T-$Nb_{1-x}Ir_xSe_2$ are in the 3+ state, the 4+–5+ state and the 2− state, respectively.

Electrical Resistivities of 1T-$Nb_{1-x}Ir_xS_2$ and 1T-$Nb_{1-x}Ir_xSe_2$

The electrical resistivities of 1T-$Nb_{1-x}Ir_xS_2$ and 1T-$Nb_{1-x}Ir_xSe_2$ were measured. The resistivity versus temperature plots are shown in Figs. 7 and 8. In both systems, the samples of the x value less than 0.1 show metallic conductivity. The samples of the x value larger than 0.1 show the semiconductivity and the values of the resistivity increase as the x value increases.

When we have explained the stability of the 1T structure in the $Nb_{1-x}Ir_xCh_2$ system, on the basis of the results of the XPS experiments, we have considered that the Ir^{3+} state is stable in the 1T lattice and is considered as a scavenger of the electrons in the host lattice. According to this scheme, the resistivity of the $Nb_{1-x}Ir_xCh_2$ should increase as the scavenger Ir atom increases. This tendency qualitatively coincides with the experimental results described above. According to this scheme, the number of carrier electrons should decrease in proportion to the concentration of Ir atoms. Consequently, the resistivity value should increase in proportion to the x value. However, the experimental resistivity value increases more rapidly than the x value. Hence, the increment of the Ir atom induces splitting of the conduction band as well as the decrement of the number of carrier electrons. This band splitting may preferentially stabilize the 1T structure over the pyrite and 2H structures.

Magnetic Susceptibility of 1T-$Nb_{1-x}Ir_xS_2$ and 1T-$Nb_{1-x}Ir_xSe_2$

The magnetic susceptibilities of 1T-$Nb_{1-x}Ir_xS_2$ and 1T-$Nb_{1-x}Ir_xSe_2$ were measured. The magnetic susceptibility versus temperature plots are shown in Figs. 9 and 10. The magnetic susceptibilities of the $Nb_{1-x}Ir_xCh_2$ indicate a weak paramagnetism or a diamagnetism. The samples of the metallic conductivity show a weak paramagnetism and the samples of the semiconductor show a diamagnetism.

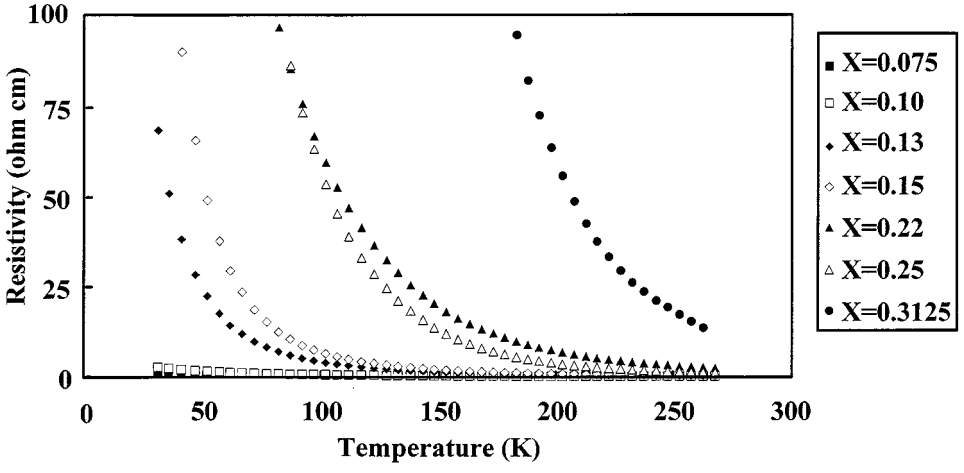

FIG. 7. Resistivity vs temperature plots of 1T-$Nb_{1-x}Ir_xS_2$.

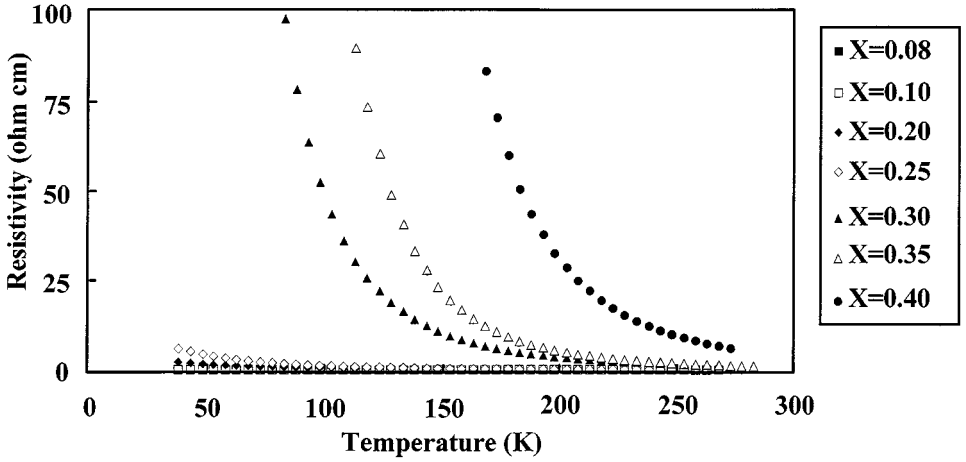

FIG. 8. Resistivity vs temperature plots of 1T-$Nb_{1-x}Ir_xSe_2$.

Therefore, a weak paramagnetism of the metallic samples may be the result of Pauli paramagnetism of the conduction electrons. The clear separation between the weak paramagnetism and the diamagnetism at the x value of 0.15 suggests that the number of the conduction electrons changes. The sample becomes a semiconductor with an x value of over 0.15. This tendency coincides with the previous experimental results of electrical conductivity.

Structural Stability of 1T Type Structure

The ground state for Ir atoms is $5d^9$. The Ir atom favors the Ir^{3+} state because of the stability of the d^6 electron configuration in the octahedral coordination. Therefore, the increment of the Ir atoms induces the decrement of the conduction electrons. Finally, the increment of the Ir atom results in the creation of the holes in the chalcogen p band. Thus, the diatomic molecule of chalcogen atoms, ch_2^{2-} is formed. The ground state for the Nb atom is $4d^5$. The Nb atom favors the electron configuration between d^0 and d^1 in the octahedral coordination. The ch atom becomes ch^{2-}, when the Nb atom has a d^1 electron configuration.

How can we predict the composition range of the 1T type structure? In the 1T structure, chalcogen atoms are discrete. Therefore, formally, the oxidation state of chalcogen atoms is considered as -2. To maintain this oxidation state, it is necessary for one metal atom to transfer four electrons to two chalcogen atoms. For the Nb atom, the maximum

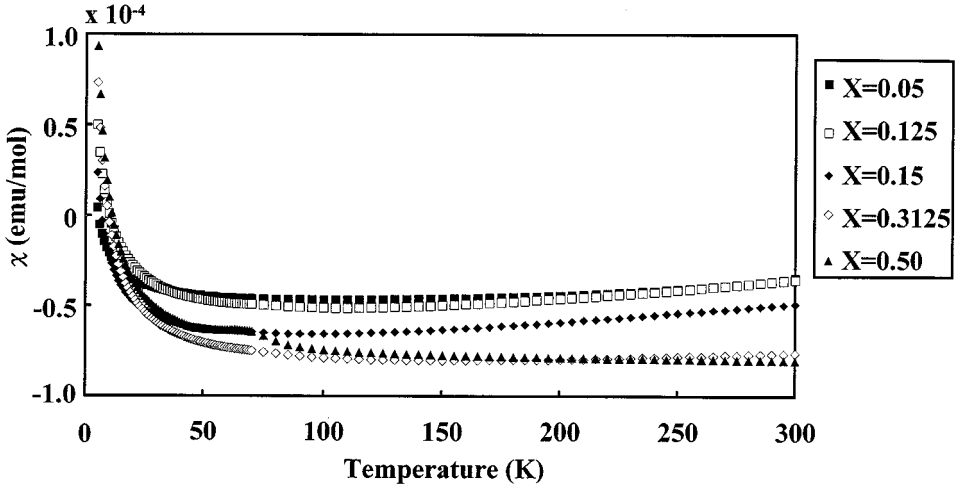

FIG. 9. Magnetic susceptibility vs temperature plots of 1T-$Nb_{1-x}Ir_xS_2$.

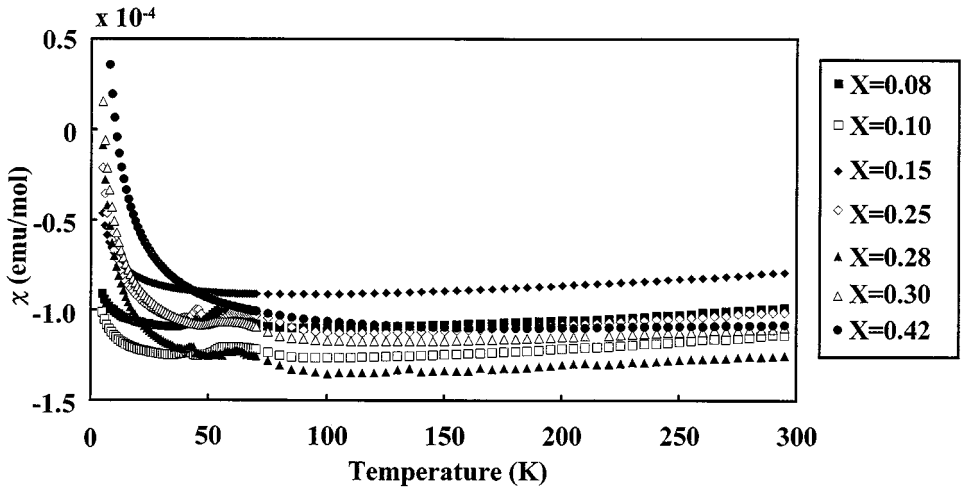

FIG. 10. Magnetic susceptibility vs temperature plots of 1T-$Nb_{1-x}Ir_xSe$.

number of transferring electrons is five, and the maximum number of transferring electrons for the Ir atom is three. Consequently, the $Nb_{1-x}Ir_xCh_2$ of the x value less than 1/2 can maintain the condition of the four electrons transferring to two chalcogen atoms. This means that the pyrite structure is not stabilized in the $Nb_{1-x}Ir_xCh_2$ of the x value less than 1/2. The Ir^{3+} state is remarkably stable in the octahedral coordination environment. Therefore, the 2H structure with the trigonal prismatic coordination metal atoms is destabilized and the 1T structure with the octahedral coordination metal atoms is stabilized.

CONCLUSIONS

(1) The present investigation revealed the phase relations of the NbS_2–IrS_2 and $NbSe_2$–$IrSe_2$ systems. Though the end members of the above systems do not crystallize into the 1T structure, a new family of 1T compounds has been prepared in the system. For the NbS_2–IrS_2 system, the 1T structure is stable in the composition range between 6 and 50 mol% IrS_2. While for the $NbSe_2$–$IrSe_2$ system, the 1T structure is stable in the composition range between 8 and 42 mol% $IrSe_2$. Also, the 1T structure is a high temperature phase and is quenchable.

(2) The electrical resistivities of the 1T-$Nb_{1-x}Ir_xS_2$ and 1T-$Nb_{1-x}Ir_xSe_2$ suggest the semiconductive property. The electrical resistivities of the above system increase as the x value increases. This behavior indicates that the number of carriers in the d band for Nb decreases as the x value increases.

(3) The magnetic susceptibilities of 1T-$Nb_{1-x}Ir_xS_2$ and 1T-$Nb_{1-x}Ir_xSe_2$ suggest the Pauli paramagnetism of conduction electrons.

REFERENCES

1. R. R. Chienell, J. C. Scanlon, and A. H. Thompson, *Mater. Res. Bull.* **10,** 1379 (1975).
2. C. R. Whitehouse, H. P. M. Rimmington, and A. A. Balchin, *Phys. Status. Solidi A* **18,** 623 (1973).
3. L. E. Conroy and K. R. Pisharody, *J. Solid State Chem.* **4,** 345 (1972).
4. S. Furuseth, K. Selte, and A. Kjekshus, *Acta Chem. Scand.* **19,** 257 (1965).
5. C. Riekel, *J. Solid State Chem.* **17,** 389 (1976).
6. D. L. Greenway and R. Nitsche, *J. Phys. Chem. Solids* **26,** 1445 (1965).
7. A. Gleizes and Y. Jeannin, *J. Solid State Chem.* **1,** 180 (1970).
8. D. L. Greenaway and R. Nitsche, *J. Phys. Chem. Solids* **26,** 1445 (1965).
9. M. Bayard and M. J. Sienko, *J. Solid State Chem.* **19,** 325 (1976).
10. K. Hayashi and M. Nakahira, *J. Solid State Chem.* **24,** 153 (1978).
11. F. Kadijk and F. Jellinek, *J. Less-Common Met.* **23,** 437 (1971).
12. E. Bjerkelund and A. Kjekshus, *Acta Chem. Scand.* **21,** 513 (1967).
13. H. P. B. Rimmington and A. A. Balchin, *J. Cryst. Growth* **21,** 171 (1974).
14. K. F. McTaggart and A. D. Wadsley, *Aust. J. Chem.* **11,** 445 (1958).
15. G. Lucovsky, R. M. White, J. A. Benda, and J. F. Revelli, *Phys. Rev. B* **7,** 3859 (1973).
16. K. D. Bronsema, G. W. Bus, and G. A. Wiegers, *J. Solid State Chem.* **53,** 415 (1984).
17. J. van Landuyt, G. van Tendeloo, and S. Amelinckx, *Acta Crystallogr. Sect. A* **31,** S85 (1975).
18. A. Prodan, F. W. Boswell, and J. M. Corbett, *Phys. Status. Solidi. A* **36,** K21 (1976).
19. F. Jellinek, G. Brauer, and H. Muller, *Nature* **185,** 376 (1960).
20. M. Marezio, P. D. Dernier, A. Menth, and G. W. Hull Jr., *J. Solid State Chem.* **4,** 425 (1972).
21. J. C. Wildervanck and F. Jellinek, *Z. Anorg. Allg. Chem.* **328,** 309 (1964).
22. V. L. Kalikhman, T. A. Lobova, and L. L. Pravoverova, *Inorg. Mater.* **9,** 826 (1973).
23. F. Jellinek, *J. Less-Common Met.* **4,** 9 (1962).
24. L. E. Conroy and K. P. Pisharody, *J. Solid State Chem.* **4,** 345 (1972).
25. E. Bjerkelund and A. Kjekshus, *Acta Chem. Scand.* **21,** 513 (1967).

26. F. Kadijk, R. Huisman, and F. Jellinek, *Rec. Trav. Chem. Pays-Bas* **83,** 768 (1964).
27. J. C. Wilderranck and F. Jellinek, *Z. Anorg. Allg. Chem.* **328,** 309 (1964).
28. J. A. Champion, *Brit. J. Appl. Phys.* **16,** 1035 (1965).
29. H. A. Al-Hilli and B. L. Evans, *J. Appl. Crystallogr.* **14,** 691 (1961).
30. V. L. Kalikhman, E. P. Gladchonko, and L. L. Pravoverova, *Inorg. Mater.* **8,** 1020 (1972).
31. J. M. Hastings, N. Elliott, and L. M. Corliss, *Phys. Rev.* **115,** 13 (1959).
32. G. Brostigen and A. Kjekshus, *Acta Chem. Scand.* **23,** 2186 (1969).
33. M. E. Staumanis, G. C. Amstutz, and S. Chan, *Amer. Mineral.* **49,** 206 (1964).
34. T. A. Bither, R. J. Bouchard, W. H. Cloud, P. C. Donohue, and W. J. Siemons, *Inog. Chem.* **7,** 2208 (1968).
35. S. Furuseth and A. Kjekshus, *Acta Chem. Scand. A* **23,** 2325 (1969).
36. H. E. King Jr. and C. T. Prewitt, *Amer. Mineral.* **64,** 1265 (1979).
37. O. Sutarno, O. Knop, and K. I. G. Reid, *Can. J. Chem.* **45,** 1391 (1967).
38. R. A. Munson, *Inorg. Chem.* **7,** 389 (1968).
39. S. Joblc, P. Deniard, R. Brec, J. Rouxel, M. G. B. Drew, and W. I. F. David, *J. Solid State Chem.* **89,** 315 (1990).
40. A. J. Jacobson and B. E. F. Frender, *J. Chem. Phys.* **52,** 4563 (1970).
41. T. A. Bither, C. T. Prewitt, J. L. Gillson, P. E. Bierstedt, R. B. Flippen, and H. S. Young, *J. Solid State Commun.* **4,** 533 (1966).
42. W. N. Stassen and R. D. Heyding, *Can. J. Chem.* **46,** 2159 (1968).
43. A. Kjekshus, T. Rakke, and A. F. Andresen, *Acta Chem. Scand. A* **33,** 719 (1979).
44. L. B. Barricelli, *Acta Crystallogr.* **11,** 75 (1958).
45. H. Zhao, H. W. Schils, and C. J. Baub, *J. Less-Common Met.* **86,** PL13 (1982).
46. A. Kjekshus, T. Rakke, and A. F. Andresen, *Acta Chem. Scand. A* **32,** 209 (1978).
47. S. Joblc, P. Deniard, R. Brec, J. Rouxel, A. Jouanneaux, and A. N. Fitch, *Z. Anorg. Allg. Chem.* **598/599,** 199 (1991).
48. J. B. Goodenough, *J. Solid State Chem.* **3,** 26 (1974).
49. Y. Maruyama, personal communication, 1989.
50. F. Izumi, *J. Cryst. Jpn.* **27,** 23 (1985).
51. W. G. Fisher and M. J. Sienko, *Inorg. Chem.* **19,** 39 (1982).
52. M. Marezio, P. D. Dernier, A. Menth, and G. W. Hull Jr., *J. Solid State Chem.* **4,** 425 (1972).
53. S. Furuseth, L. Brattas, and A. Kjekshus, *Acta Chem. Scand.* **27,** 2367 (1973).
54. R. Nyholm and N. Martensson, *Solid State Commun.* **40,** 311 (1981).
55. R. Nyholm, A. Berndtsson, and N. Martensson, *J. Phys. C* **13,** L1091 (1980).
56. R. Riga and J. J. Verbist, *J. Chem. Soc., Perkin Trans. II* **1983,** 1545 (1983).
57. D. Cahen, P. J. Ireland, L. L. Kazmerski, and F. A. Thiel, *J. Appl. Phys.* **57,** 4761 (1985).